Estimation of Synchrophasor Parameters in the Presence of 3rd & 5th Harmonics and White Gaussian Noise

Kassaye Gizaw(✉), Alganesh Ygzaw, Belachew Bantyirga, and Habtemariam Aberie

Bahir Dar Institute of Technology, Bahir Dar, Ethiopia

Abstract. Nowadays, power systems, particularly distribution networks, often operate close to their stability limit due to the rapid growth of new customers and inauguration of industrial sectors. Though the advancement of renewable energy sources (RESs) and Flexible Alternating Current Transmission (FACT) devices are the right solutions to meet these demands, they increase the network's complexity and dynamic behavior. To solve these complexities, introducing advanced controllers that are fast, accurate, and have a reliable synchronization method is the most effective solution. On this basis, one of the foremost promising technologies that constitute the backbone of wide-area and local monitoring systems in real-time is the Phasor Measurement Units (PMU) device. Thus, in this paper, the synchrophasor estimation (SE) algorithm, which is the main component to build up a PMU, is developed using the iterative interpolated DFT technique. Even if the analyzed interferences are two harmonics (3rd and 5th), the developed algorithm can work for any type and number of interferences. Based on the simulation result demonstration, the algorithm can effectively estimate the amplitude, phase, and frequency within the maximum error of 0.039, 0.002, and 0.0001.

This research work can solve various interrelated problems of electrical utilities for those lacking a tool that can trace the system at proper time snapshot like in our country Ethiopia.

Keywords: Discrete Fourier transform (DFT) · SE algorithm

1 Introduction

Nowadays power systems often operate close to their stability limit due to the rapid growth of new customers and inauguration of industrial sectors in the existing distribution networks. Even if the advancement of RESs and FACT devices are the best solutions to meet these demands, they increase the complexity and dynamic behavior of the system [1].

Also, to enhance the efficiency of power system networks, they require the successful coordination of real-time processes such as real-time power flows and demand-side response along with the requirement of advanced technologies like grid control devices, smart meters, and agent-based distributed controls [2, 3].

M. A. Delele et al. (Eds.): ICAST 2020, LNICST 384, pp. 215–230, 2021.
https://doi.org/10.1007/978-3-030-80621-7_16

To solve these problems, investing in grid reinforcement can be the first viable option. However, this mechanism does not enable the control of flexible resources available in active distribution networks (ADNs). On top of that, it also involves a significant increase in capital expenditure. Another option that considerably reduces the required investments compared to the previous one is introducing advanced controllers that are fast, accurate, and have reliable synchronization methods [1]. These infrastructures are better than present solutions such as Supervisory Control and Data Acquisition (SCADA) and the distribution automation system (DAS). Within this context, one of the foremost promising technologies that constitute the backbone of wide-area and local monitoring systems in real-time is the Phasor Measurement Units (PMU) device.

The scientific literature in the field of synchrophasor is relatively recent. Based on the adopted signal model, its estimation algorithm can be a static or dynamic model [4].

Static signal model-based SE algorithms are the most common because of their low computational complexity and estimation accuracies. The majority of these methods are based on the direct implementation of the DFT due to its relatively low computational complexity, the capability to reject close by harmonics, and its ability to separate and identify the fundamental parameters of the signal [5–7]. Some methods have good performance in SE like a phase-locked loop (PLL) but they are poor in parameter selection [8]. Even though the method proposed in [7] tries to compensate for the long-range spectral leakage of the negative image of the main tone, it does not account for the spectral interference produced by tones other than the fundamental tone. The method presented in [9] satisfies the IEEE P- and M-Class Compliant test of PMUs.

Nevertheless, it doesn't consider the effects of odd harmonics like third and fifth-order harmonics, in which its analysis is vital for developing countries like Ethiopia. Some window-based methods may require an integral sample in each window [10]. However, non-integer samples in a window are common in reality because of some off-nominal components which can result in errors in the DFT. Some algorithms may have good harmonic rejection capability, but they are computationally complex and susceptible to noise [11, 12].

1.1 Phasor, Synchrophasor, and Phase Measurement Unit

During normal operation of a power system, voltage and current waveforms are usually modeled as follows.

$$x(t) = A_o.\cos(\omega_o t + \varphi_o),\ \ ==>\ \omega_o = 2\pi f_o t \tag{1}$$

Phasor Definition: The electrical systems in a sinusoidal steady-state are simplified by the adoption of a phasor transformation.

It allows representing a sinusoidal function of time like the one expressed by an Eq. (1) with a single complex constant and vice versa. Therefore, the above time-domain signal can be represented in the phasor form by transforming it into a complex exponential via Euler's formula [13].

$$x(t) = A.\cos(\omega t + \varphi) = \mathrm{Re}\left\{A\Big/\sqrt{2}e^{j(\omega t+\varphi)}\right\} = \mathrm{Re}\left\{A\Big/\sqrt{2}e^{j\omega t}e^{\varphi}\right\} \tag{2}$$

By assuming everything in the circuit remains at a steady sinusoid of the same frequency, it is rational to associate the sinusoid *x(t)* to the complex number *X* and call it phasor.

$$X = |X|.e^{\varphi} \quad \text{(in a polar form)}.$$

$$\text{Where } |X| = A\Big/\sqrt{2}, \text{ is the RMS value.}$$

$$x(t) \rightleftarrows X = |X|.e^{\varphi} = |X|[\cos\varphi + j\sin\varphi]$$

$$|X|.e^{\varphi} = X_r + jX_i \text{ (in a rectangular form) and arg } (X) = \varphi = \tan^{-1}\left(X_i\Big/X_r\right).$$

Synchro Phasor: the signal *x(t)* in the above Eq. (1) can be represented as a synchrophasor using the complex function *X(t)* with amplitude *A(t)* and phase $\psi(t)$ of the main tone respectively, being *t* the UTC time-reference.

$$\begin{aligned} x(t) \rightleftarrows X(t) &\triangleq A(t).e^{j\psi(t)} \\ &= A(t).e^{j(2\pi f(t)+\varphi)} \\ &= A(t)[\cos(\omega t + \varphi) + j\sin(\omega t + \varphi)] \end{aligned} \tag{3}$$

where *A(t)* and $\psi(t) = 2\pi f(t) + \varphi$ are the instantaneous peak amplitude and phase of the main tone of *x(t)*. The representation of this function on the complex plane is a complex number that describes a circular trajectory with an angular radius ω, amplitude *A*, and its initial phase φ.

1.2 PMU Technology in Distributions System

The prototypes of the modern synchronized "phasor measurement units" (PMUs) using GPS were built at Virginia Tech in the early 1980s, and it was commercial manufacture in1991 [14, 15].

According to the IEEE Standard. C37.118.1-2011, PMU is a device that estimates the synchro phasors such as frequency and rate of change of frequency (ROCOF) of the voltage/current waveforms depending on a common UTC reference [5] (Fig. 1).

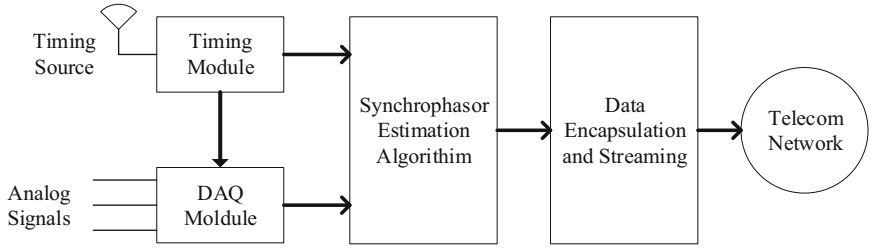

Fig. 1. Basic block diagrams of PMUs [8]

PMU technology has been initially developed to estimate transmission network parameters. Eventually, it has emerged as a potential control of ADNs and microgrids and a candidate for real-time monitoring [15].

By using synchrophasor technology, operators can monitor grid dynamics and reliability metrics. Also, they can identify and diagnose system problems, system stresses, oscillations, and other abnormal situations.

These enable them to take proactive actions to prevent or to reduce the footprint of blackouts and enable faster recovery after events [16].

The following Fig. 2 shows the performance comparison of PMU and SCADA when a voltage disturbance occurred on the Oklahoma power grid on April 5, 2011 [17].

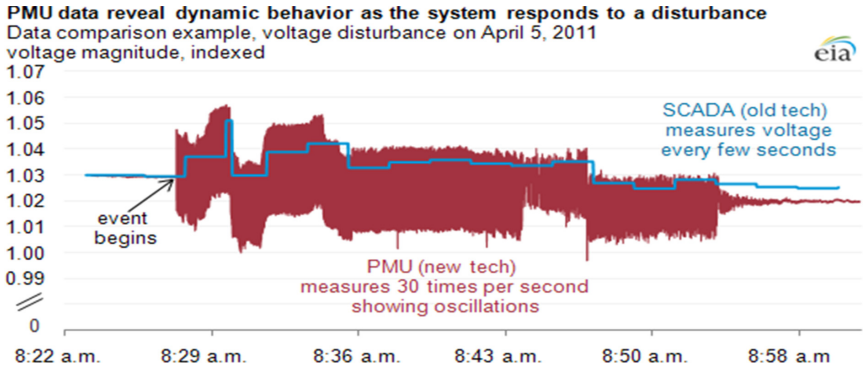

Fig. 2. Performance comparison of PMU vs. SCADA measurements [17]

In the above figure, it is clearly depicted that PMU measurements are very precise to captures the dynamic conditions. In contrast, SCADA measurement is not able to observe the dynamic characteristics of the power system as it relies on steady-state power flow analysis. As a result, it is not possible to take proper control action to alleviate the oscillation.

The other problem is that SCADA technology only gives the magnitude of different electrical quantities like voltages and currents. In the AC network, there is one essential parameter apart from the magnitude that is the angle which is a key indicator of the system stress. If we rely only on the magnitude of information without including the angle, we might lose some information and monitor the system wrongly [13]. These can, in turn, cause serious interrelated problems in a power system like relay misoperation, incorrect coordination between power equipment and it may also lead to a blackout.

2 DFT Theory and Its Effects

DFT is one of the most efficient tools to extract the frequency content of a finite and discrete signal sequence, which is obtained from the periodic sampling of a continuous time-domain signal.

PMU is nothing, but it is a name of a device where a robust algorithm can estimate the phasors of electrical quantities deployed on in its microcontroller unit, which makes

it very smart and expensive [7]. A direct implementation DF-based SE algorithm is proposed in almost all of the previously reviewed literature due to low computational complexity, capable to isolate and identify the main tone parameters, good rejection of near harmonics, and accurate in steady-state and dynamic conditions [18]. Nevertheless, these qualities come with non-negligible drawbacks mainly caused by DFT computation, such as aliasing and spectral leakage.

Aliasing: is a problem that is related to the finite BW of the data acquisition system concerning the signal that we are interested to track. To be able to correctly reconstruct the signal *x(t)* from *x[n],* it must be sampled at a sampling rate F_s that must be at least two times higher than the maximum frequency component contained in the original spectrum *X(f)* (Nyquist–Shannon theorem) [7]. It is usually corrected by using an anti-aliasing filter, but this may introduce a phase shift all over the spectrum that has to be compensated. The second mechanism to get rid of the problem is to select a higher sampling frequency (F_s) than F_m (maximum frequency component of our signal) which is unknown in the real signal. So, in the power system of such type applications, it is usually set the sampling frequency at the value of 10^{th} of kHz because, at this frequency, typically don't have any other interfering components except transient. In the power system, the highest harmonic we can get is 25^{th} harmonics, which is 1.25 kHz for 50 Hz fundamental frequency [19]. So, if the sampling frequency is set to 10 kHz, 15 kHz, or 100 kHz this hypothesis seems good than the first case (Fig. 3).

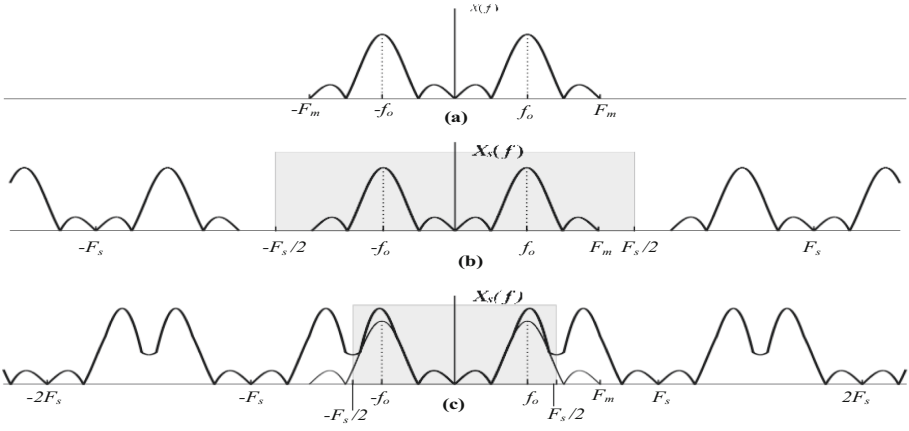

Fig. 3. Effects of aliasing [5]

Spectral Leakage: After the sampling of the original signal *x(t)*, it must be grouped in portions to be analyzed by the DFT. If the fundamental frequency (f_o) is not an integer multiple of frequency resolution (incoherent sampling), the zero crossings of the translated *sinc* functions will not happen exactly at multiples of 1/T and all the DFT indexes will not be an integer. As a result, we start to see several bins as they exhibit non-zero projection on the entire basis set due to the smearing frequency components as shown in Fig. 4. Even though most of the spectrum energy (bins that are adjacent to

f_o) will still be concentrated around, the highest frequency bin is not located precisely at the f_o. Spectral leakage can be short term or long term.

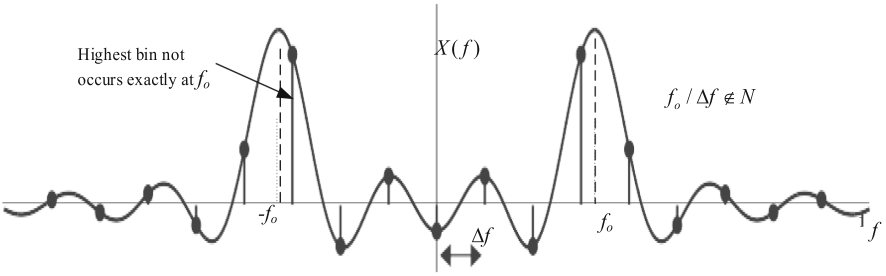

Fig. 4. Graphical representation of spectral leakage [5]

Short-term arise from the effects of the main lobe width of the FT of the adopted window which in turn makes very difficult in identifying the "true" maximum of a specific portion of the DFT spectrum.

Whereas the effect caused by the side-lobes (i.e., the "tails") of the FT of the adopted window is referred to as *long-term.* If it is not properly compensated by windowing, an additional source of error is associated with the presence of cross interaction between spectrum tones that are very close to each other, the so-called spectral interference occurs (Fig. 5).

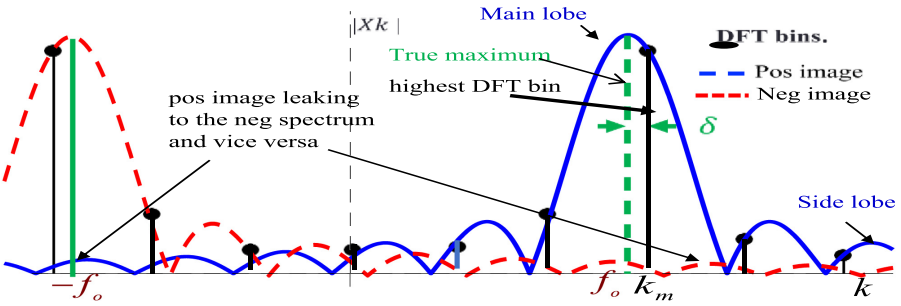

Fig. 5. Main and side lobes [9]

2.1 DFT Based SE Algorithms

Classical DFT-based SE. A trivial DFT-based SE algorithm approach estimates the parameters of the main DFT tone directly from the position of a local DFT maximum within a specific frequency range. It is based on the assumption that the maximum DFT bin lies precisely at the fundamental frequency. But if the window does not contain an integer number of periods of the signal *x[n],* leakage occurs, and the main tone of the signal is located between two consecutive DFT bins as shown in Fig. 6.

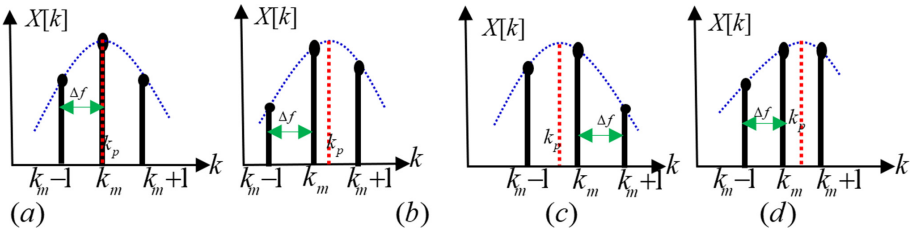

Fig. 6. Possible location of the three highest DFT bins

The pseudo-code of a trivial DFT-based synchrophasor estimation algorithm.

1. Sample the input signal x (t) → x[n]at sampling rate Fs.
2. Apply the rectangular window w_r *(n)* to *x[n];*
3. Compute the DFT of w_r *(n)* · *x[n];*
4. Apply a maximum search technique to find the DFT bin with the highest amplitude $|X(k_m)|$; being k_m is the index of the highest DFT bin of the spectrum.
5. Return estimated value of amplitude, phase, and frequency of $X(k_m)$;
   $f = k_m \Delta f, \quad A = |X(k_m)|, \quad \varphi = \angle X(k_m)$
6. End procedure

The Interpolated-DFT Technique is a technique that allows estimating the main tone spectrum location by calculating the abscissa of the maximum of an interpolation curve of the DFT spectrum under the fulfillment of some essential assumptions. These assumptions are sufficiently higher sampling frequency than F_m, time-invariant parameters characterize the input signal, and the bins that are going to interpolated are only generated by the positive image of the tone.

Thus, to satisfy the first two assumptions, the window length containing a few periods of a fundamental tone and the sampling rates selected in a few kilohertz, respectively. Nevertheless, if the window includes few periods only, the DFT spectrum's energy will be concentrated in the lower frequency range; thereby, the positive and negative images of the main tone of the spectrum become relatively very close to each other. During this condition, the third assumption may not be fulfilled. Because in the case of incoherent sampling, the negative image tails of the main tone leaks into its positive spectrum, thereby bias the DFT bins used to perform the interpolation.

Thus, to solve this problem, the IpDFT starts its analytical analysis from the following four equations describing Hanning (Hann) window in the continuous-time domain, discrete-time domain, Fourier transforms and its DFT, respectively.

$$w_h(t) = 0.5(1 + \cos(2\pi t/T)) \tag{4}$$

$$w_H(n) = 0.5(1 - \cos(2\pi n/N)), \; n \in [0, N-1] \tag{5}$$

$$W_H(\omega) = -0.25 \cdot D_N(\omega - 2\pi/N) + 0.5 \cdot D_N(\omega) - 0.25 \cdot D_N(\omega + 2\pi/N) \tag{6}$$

$$W_H(k) = -0.25D_N(k-1) + 0.5D_N(k) - 0.25D_N(K+1) \tag{7}$$

Where $D_N(\omega)$ the Dirichlet kernel (FT of the rectangular window) and its DFT is:

$$D_N(k) = e^{-j\pi k(N-1)/N} \frac{\sin(\pi k)}{\sin(\pi k/N)}, \quad k \in [0, N-1] \tag{8}$$

Let's consider the finite sequence (9) obtained by sampling with a sampling rate of a continuous waveform *x(t)* characterized by a single frequency component at frequency:

$$x(n) = A\cos(2\pi f_o n T_s + \varphi), \quad 0 \le n \le N-1 \tag{9}$$

Where A is signal's amplitude, f_o is the signal's frequency in Hertz. Then its spectrum can be expressed in terms of its positive and negative image as follows.

$$\begin{aligned} X(f) &= X^+(f) + X^-(f) \\ &= \frac{A}{2}e^{j\psi}W_H(f - f_o) + \frac{A}{2}e^{-j\psi}W_H(f + f_o) \end{aligned} \tag{10}$$

Being $W_H(f)$ the Fourier transform of the Hanning window, A and ψ the amplitude and instantaneous phase of the signal *x(t)* respectively.

By letting the effects of leakage are properly compensated by windowing, it is reasonable to neglect the long-range spectral leakage produced by the negative spectrum image on the positive frequency range thereby assumption three satisfies which is approximated mathematically as:

$$X(k) \approx X^+(k), \qquad 0 \le k \le N/2 \tag{11}$$

These for the Hanning window, the fractional term δ can be estimated starting from the ratio between the two highest bins *X(km)* and *X (km + ε)* that, can be approximated as follows [62].

$$\frac{X(k_m + \varepsilon)}{X(k_m)} \approx \frac{W_H\left((\varepsilon - \delta)\cdot 2\pi/N\right)}{W_H(-\delta \cdot 2\pi/N)} \tag{12}$$

Where $W_H(\cdot)$ is the FT of the Hanning window, which is approximated as:

$$|W_H(\omega)| \approx \left|\sin(\frac{\omega N}{2})\right| \cdot \left|\frac{-0.25}{\sin(\frac{\omega}{2} - \frac{\pi}{N})} + \frac{0.5}{\sin(\frac{\omega}{2})} + \frac{-0.25}{\sin(\frac{\omega}{2} + \frac{\pi}{N})}\right| \tag{13}$$

$$\varepsilon = \begin{cases} 1 & \text{if} |X(k_m+1)| > |X(k_m-1)| \\ -1 & \text{if} |X(k_m+1)| < |X(k_m-1)| \end{cases} \tag{14}$$

By replacing (14) in (12) and recalling that $\lim_{x\to 0}\sin(x) = x$, after simplification we get:

$$\frac{X(k_m + \varepsilon)}{X(k_m)} = \left|\frac{0.5}{\delta(\delta-\varepsilon)(\delta-2\varepsilon)}\right| \left|\frac{\delta(\delta+1)(\delta-1)}{-0.5}\right| \Leftrightarrow = \left|\frac{\delta+\varepsilon}{\delta-\varepsilon}\right|$$

Therefore, the frequency correction δ becomes:

$$\delta = \varepsilon \frac{2|X(k_m + \varepsilon)| - |X(k_m)|}{|X(k_m)| + |X(k_m + \varepsilon)|} \tag{15}$$

Then IpDFT technique computes the initial waveform parameters (i.e., its frequency, amplitude, and phase) as follows:

$$\begin{aligned} f &= (k_m + \delta)\Delta f \\ A &= |X(k_m)| \left| \frac{\pi\delta}{\sin(\pi\delta)} \right| \left| \delta^2 - 1 \right| \\ \varphi &= \angle X(k_m) - \pi\delta \end{aligned} \tag{16}$$

2.2 The Iterative IpDFT Technique

IpDFT technique tries to compute the main tone parameters by letting the DFT bins are only generated from the positive image of the spectrum. Nevertheless, this assumption is not always the case and the bins may influence by the negative image of the main tone itself and other interfering tones like harmonics. Thus, the i-IpDFT technique tries to eliminate any interferences iteratively, and finally, it estimates the fundamental tone parameters.

So, to start the mathematical analysis of the i-IpDFT, let us consider a 3rd harmonic is added in the signal described by the Eq. (9). Hence, the highest and second-highest DFT bins, are used to estimate δ according to (15), they can be expressed as:

$$X(k_m) = \frac{1}{B}\left[\frac{A}{2}e^{j\varphi} \cdot W(-\delta) + \frac{A}{2}e^{-j\varphi} \cdot W(2k_m + \delta)\right] + X\left(K_{m,3}\right) \tag{17}$$

$$X(k_m + \varepsilon) = \frac{1}{B}\left[\frac{A}{2}e^{j\varphi} \cdot W(\varepsilon - \delta) + \frac{A}{2}e^{-j\varphi} \cdot W(2k_m + \varepsilon + \delta)\right] + X\left(K_{m,3} + \varepsilon\right) \tag{18}$$

Where $X(K_{m,3})$ and $X(K_{m,3} + \varepsilon)$ are the contribution of third harmonics for the first and second highest DFT bins respectively.

$$X(K_{m,3}) = \frac{A_3}{2B}\left(e^{j\varphi_3} \cdot W(-\delta_3)\right) + \frac{A_3}{2B}\left(e^{-j\varphi_3} \cdot W(2k_{m,3} + \delta_3)\right) \tag{19}$$

$$X(K_{m,3} + \varepsilon) = \frac{A_3}{2B}\left(e^{j\varphi_3} \cdot W(\varepsilon - \delta_3)\right) + \frac{A_3}{2B}\left(e^{-j\varphi_3} \cdot W(2k_{m,3} + \varepsilon + \delta_3)\right) \tag{20}$$

The second terms after the addition sign in the Eqs. (17) to (20) are spectral interference coming from the negative spectrum image of the corresponding tones. Then, these estimations can be subtracted from the original DFT bins to reduce the spectral interference so that the positive image of the spectrum mostly generates the compensated DFT bins. These compensated DFT bins are used to update the value of delta in the Eq. (15) and which again updates the tone parameters which is iterated for defined number iterations or performed until a given convergence criterion is achieved. Additionally, this process can be similarly used to eliminate any near harmonic components.

As a procedure, the effect of the main tone's negative image has to be compensated first iteratively, which affects highly before we analyze the contribution of harmonic components. Then the effects of harmonics can be analyzed one by one starting from the first harmonic which is closer to f_o. The estimated frequency can be expressed as;

$$f_o = k_{peak}\,\Delta f\,. \tag{21}$$

Where k_{peak} can be expressed as:

$$k_{peak} = k_{\max} + \delta, \quad -0.5 \le \delta \le 0.5 \Rightarrow \begin{cases} k_{peak} = k_{\max}, (\delta = 0), \rightarrow \text{coherent, no leakage} \\ \mathrm{k}_{peak} \neq k_{\max}, \ (\delta \neq 0) \rightarrow \text{incoherent, leakage} \end{cases}$$

Being k_m the index of the DFT bin characterized by the highest amplitude and δ is a fractional correction term.

Incoherent sampling, the highest DFT bin of the signal's spectrum is located at the maximum of the window lobe that can be used to estimate the frequency of the signal.

Figure 7 shows the general flow chart of the work. The first step is acquiring the input signal through current and potential transformers. Once the signal is received it has to be sampled at the desired sampling rate Fs and then it must be clustered in portions to be analyzed by the DFT which is called windowing. After the windowing, the first three DFT maximums has to be computed based on the trivial and IpDFT approach. Then after the errors in finding DFT maximums can be minimized by eliminating the effect of negative image spectral interference of the corresponding tone by using a technique called e-IpDFT. Once the effect of negative image interferences is eliminated to endurable value the spectral energy is computed which is vital to quantify the effect of other interferences. If the spectral energy is above some threshold value, the true parameters of all interferences are going to be estimated and subtracted from the original DFT spectrum iteratively to increase the accuracy of estimated fundamental tone parameters.

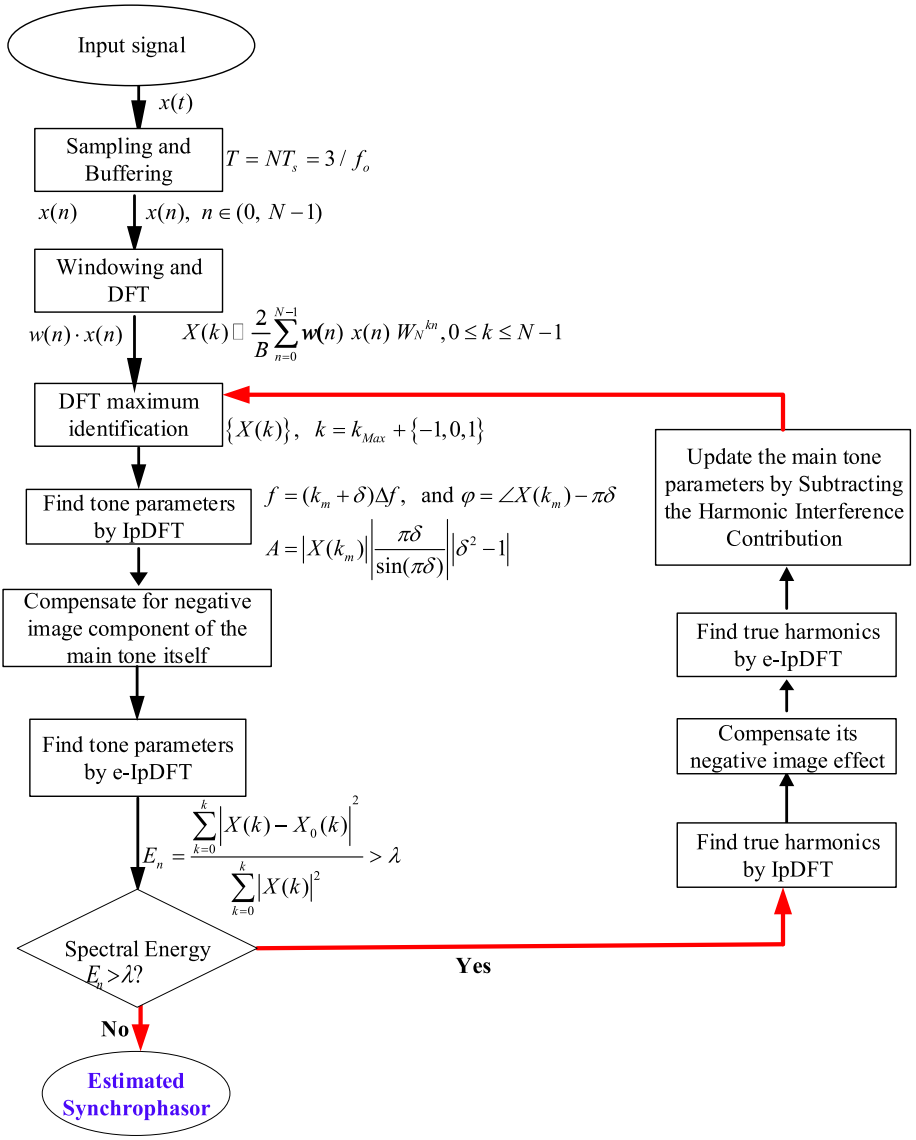

Fig. 7. General flow chart

3 Simulation Results and Discussion

For all scenarios, the fundamental phase is taken as 1.0471975511966 rad and the amplitude of the 3rd and the 5th harmonics are taken as 10% & 1% of the corresponding fundamental amplitude. The white Gaussian noise is considered as 60 dB.

3.1 Estimated Parameters When the Fundamental Frequency is Below 50 Hz

For frequency below 50 Hz, $A_o \& f_o$, are randomly generated as 9.64310742178912 and 48.7340275 Hz respectively whereas the phase of the 3rd and 5th harmonics are assumed to be 0.130855503942357 rad and 0.00727912525993756 rad respectively.

The Frequency domain format of the windowed signal is shown in Fig. 8 (a). From this figure, the three signals of the spectrum which are the fundamental, 3rd, and 5th harmonics are shown. The classical DFT algorithm estimates the frequency exactly the index corresponding to the highest DFT bin which is 50 Hz in this case. Thus, to estimate the exact fundamental frequency the interference and the leakages need to be considered in Fig. 8 (b). The interferences around the fundamental tone from Fig. 8 (b) are occurred due to the trivial difference between the actual amplitude and the estimated one.

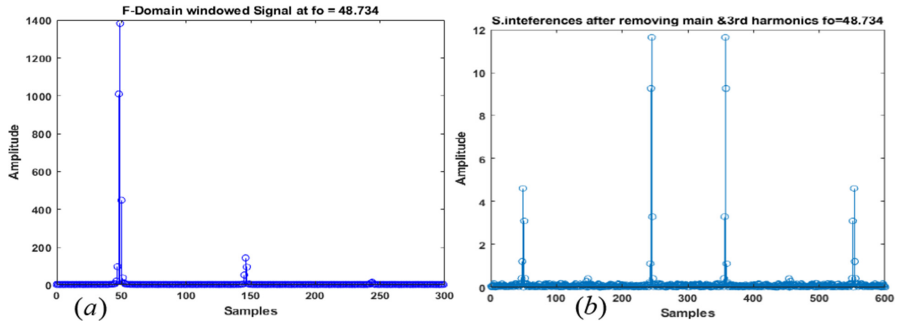

Fig. 8. (a) Frequency domain of windowed signal, and (b) interference spectrum after subtracting the main tone and 3rd harmonics, $fo = 48.7340275031078$

Lambda λ in Fig. 7 is set to 0.0001 for all scenarios where it is used to activate the algorithm to compensate for the interferences when their effect is significant. The errors in Fig. 9 are obtained after an elven iteration and the value of *En* at this iteration is found to be 0.000013454306809327.

3.2 Estimated Parameters When the Fundamental Frequency is 50 Hz

At a frequency of 50 Hz, A_o is taken as 10 whereas the phase of the 3rd and 5th harmonics are assumed to be 0.466031331142832 rad and 1.2263488297847 rad respectively as they are generated dynamically for each scenario.

It is already discussed that when the time domain signal is an integer multiple of the sampling frequency there will be coherent sampling thereby the maximum DFT bin is located almost in the middle of the other two bins which are nearly equal in amplitude as shown in Fig. 10 (a). As a result; the smearing frequency components reduced and the algorithm able to estimate the fundamental parameters in small iterations (Table 1).

Figure 10 (b) depicts the negative image leakages of the main tone for all DFT bins that have to be compensated for each positive image bins.

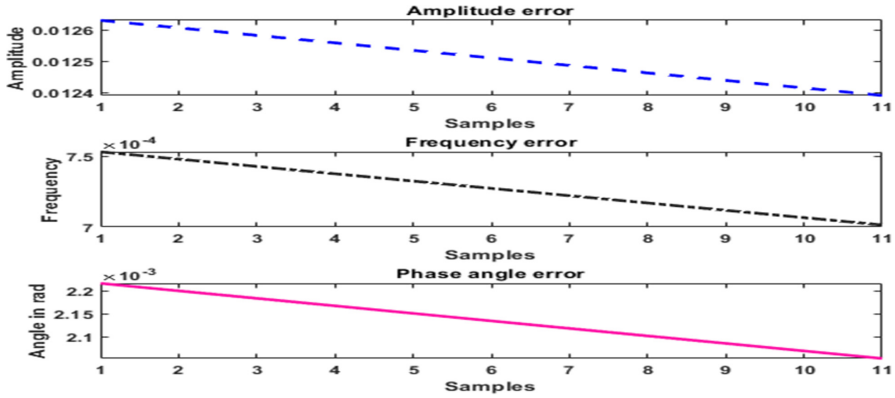

Fig. 9. Error in amplitude, phase, and frequency, $fo = 48.7340275031078$ Hz

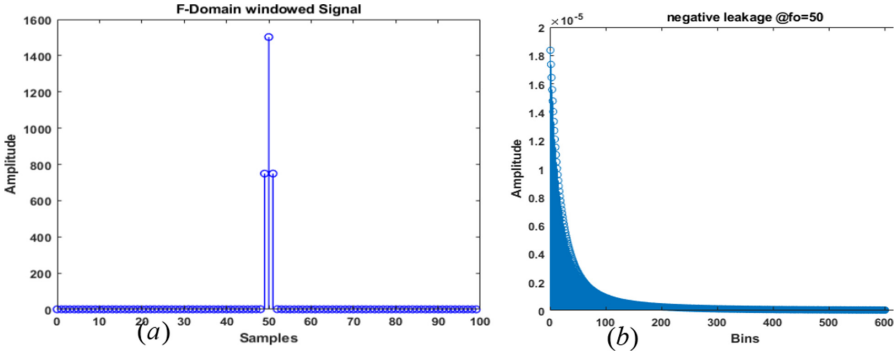

Fig. 10. (a) Frequency domain of windowed signal, and (b) magnitude of negative leakage of the main tone, $fo = 50$Hz

Table 1. Errors in amplitude, frequency, and phase $fo = 50\ Hz$

Iteration	1	2
Amplitude error	0.03914	0.03914
Frequency error	0.000142	0.000141
Phase angle error	0.002917	0.002915

3.3 Estimated Parameters When the Fundamental Frequency is Above 50 Hz

The algorithm is also tested when the real frequency is above the nominal value which is 50 Hz. The amplitude and the real frequency are assumed to be 9.48665553956213 and 51.6415849459746 Hz respectively. Similarly, the phase angle of the harmonics is randomly generated and their instant values for this scenario are 1.05155216148873 rad and 2.03957598834408 rad for 3rd and 5th harmonics respectively.

The classical DFT estimates the frequency 52 Hz which is the index of the highest DFT bin from Fig. 11 (a) but it is not the fundamental or the real frequency. Figure 11 (b) presents the interference after removing the main tone and 3rd harmonics and it is shown that there is an interference around the fundamental component other than the 5th harmonics which is due to the difference between true and estimated amplitude..

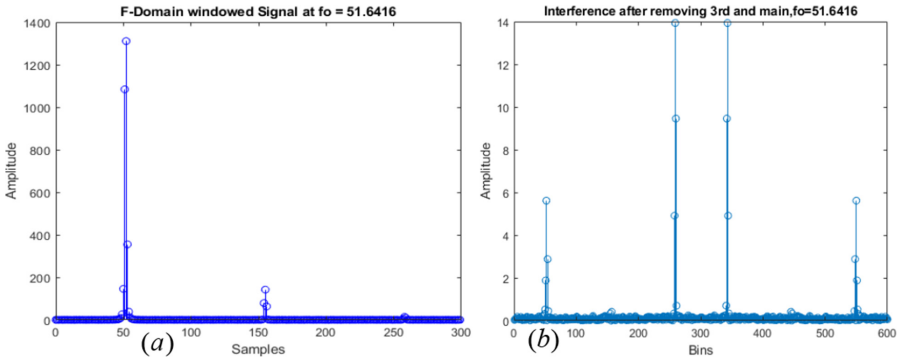

Fig. 11. (a) the spectrum of the windowed signal and (b) interferes spectrum after subtracting the main tone and 3rd harmonics (Fig. 12).

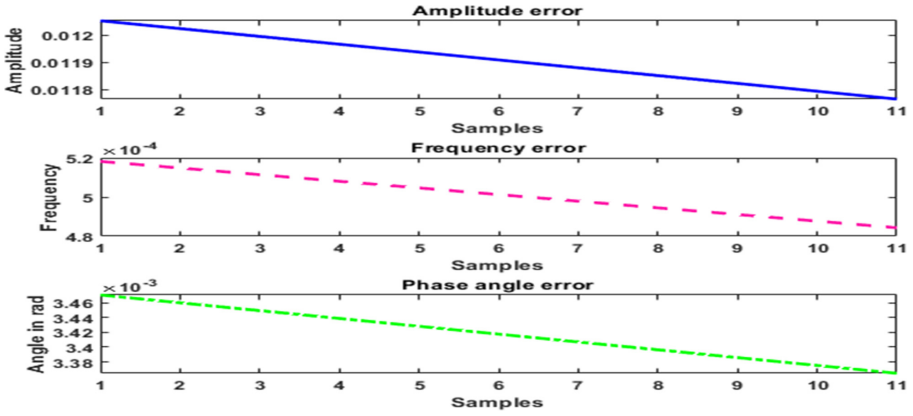

Fig. 12. Errors in amplitude, frequency, and phase, $fo = 51.6415849459746$ Hz

4 Conclusion

In this research work, an efficient method called the i-IpDFT technique has been anticipated to estimate the phasor parameters of the fundamental tone at three different instant of input signal parameters. The simulation results show that the i-IpDFT SE technique is robust and solves the limits of the IpDFT technique when estimating the parameters of a signal corrupted by interference signals and leakage generated by them and by the

main ton itself. The errors in all scenarios are within the limit and acceptable for further applications of the power system, especially for distribution systems where most of its operations are not going on a nominal value as they are typically corrupted by non-linear loads and other factors.

Thus, considering the effects of noise and odd harmonics like third and fifth-order harmonics to know the real or fundamental parameters of the power system is vital for developing countries like Ethiopia.

References

1. Frigo, G., Derviskadic, A., Zuo, Y., Paolone, M.: PMU-based rocof measurements: uncertainty limits and metrological significance in power system applications. IEEE Trans. Instrum. Meas. **68**, 3810–3822 (2019). https://doi.org/10.1109/TIM.2019.2907756
2. Alzaareer, K., Saad, M.: Real-time voltage stability monitoring in smart distribution grids. IEEE Int. Conf. Renew. Energy Pow. Eng. REPE **2018**, 13–17 (2018). https://doi.org/10.1109/REPE.2018.8657671
3. Romano, P., Paolone, M., Arnold, J., Piacentini, R.: An interpolated-DFT synchrophasor estimation algorithm and its implementation in an FPGA-based PMU prototype. IEEE Pow. Energy Soc. Gen. Meet. (2013). https://doi.org/10.1109/PESMG.2013.6672906
4. Castello, P., Lixia, M., Muscas, C., Pegoraro, P.A.: Impact of the model on the accuracy of synchrophasor measurement. IEEE Trans. Instrum. Meas. **61**, 2179–2188 (2012). https://doi.org/10.1109/TIM.2012.2193699
5. Milano, F.: Advances in Power System Modelling, Control, and Stability Analysis (2016)
6. Thilakarathne, C., Meegahapola, L., Fernando, N.: Static performance comparison of prominent synchrophasor algorithms. In: 2017 IEEE Innovative Smart Grid Technologies - Asia Smart Grid Smart Community, ISGT-Asia 2017, pp. 1–6 (2018). https://doi.org/10.1109/ISGT-Asia.2017.8378392
7. Romano, P., Paolone, M.: Enhanced interpolated-DFT for synchrophasor estimation in FPGAs: theory, implementation, and validation of a PMU prototype. IEEE Trans. Instrum. Meas. **63**, 2824–2836 (2014). https://doi.org/10.1109/TIM.2014.2321463
8. Cai, X., Wang, C., Kennel, R.: A fast and precise grid synchronization method based on fixed-gain filter. IEEE Trans. Ind. Electron. **65**, 7119–7128 (2018). https://doi.org/10.1109/TIE.2018.2798600
9. Derviskadic, A., Romano, P., Paolone, M.: Iterative-interpolated DFT for synchrophasor estimation: a single algorithm for P- and M-class compliant PMUs. IEEE Trans. Instrum. Meas. **67**, 547–558 (2018). https://doi.org/10.1109/TIM.2017.2779378
10. Li, H.: Frequency estimation and tracking by two-layered iterative DFT with re-sampling in non-steady states of power system. EURASIP J. Wirel. Commun. Netw. **2019**(1), 1–19 (2019). https://doi.org/10.1186/s13638-018-1320-1
11. Kim, D.I., Chun, T.Y., Yoon, S.H., Lee, G., Shin, Y.J.: Wavelet-based event detection method using PMU data. IEEE Trans. Smart Grid. **8**, 1154–1162 (2017). https://doi.org/10.1109/TSG.2015.2478421
12. Maharjan, S., Peng, J.C.H., Martinez, J.E., Xiao, W., Huang, P.H., Kirtley, J.L.: Improved sample value adjustment for synchrophasor estimation at off-nominal power system conditions. IEEE Trans. Pow. Deliv. **32**, 33–44 (2017). https://doi.org/10.1109/TPWRD.2016.2586946
13. Palsodkar, S.S., Date, T.N.: Comparison of DFT and space vector method for synchrophasor measurement. In: Proc - 2018 4th International Conference on Computing Communication Control and Automation, ICCUBEA 2018, pp. 1–6 (2018). https://doi.org/10.1109/ICCUBEA.2018.8697374

14. Nuthalapati, S.(N.D.R.) (ed.): Power System Grid Operation Using Synchrophasor Technology. PEPS, Springer, Cham (2019). https://doi.org/10.1007/978-3-319-89378-5
15. Penshanwar, M.K., Gavande, M., Satarkar, M.F.A.R.: Phasor measurement unit technology and its applications-a review. In: International Conference on Energy Systems and Applications, ICESA 2015, vol. 17, pp. 318–323 (2016). https://doi.org/10.1109/ICESA.2015.7503363
16. Bennett, J.M.: Towards ethnorelativism: a developmental model of intercultural competence. Springer, Heidelberg (1986)
17. EIA: U.{S}.{Energy}{Information}{Administration}({EIA}) (2015). http://www.eia.gov/. Accessed 22 July 2019
18. Affijulla, S., Tripathy, P.: Development of phasor estimation algorithm for P-class PMU suitable in protection applications. IEEE Trans. Smart Grid **9**, 1250–1260 (2018). https://doi.org/10.1109/TSG.2016.2582342
19. Soni, M.K., Soni, N.: Review of causes and effect of harmonics on power system. Int. J. Sci. Eng. Technol. Res. **3**, 214–220 (2014)